ASC24- 1LPo1I-02

Influence of Critical Current Defect on Operation, Quench Detection and Protection of a Conduction-Cooled Pancake REBCO Coil

M. Wozniak, E. Schnaubelt, S. Atalay, B. Bordini,
J. Dular, T. Mulder, E. Ravaioli and A. Verweij

***Abstract*— High-temperature superconductor (HTS) coated conductors (CC) are often wound into pancake coils with electrical insulation in-between the turns. The copper terminals are used for current injection and conduction cooling. An inherent variation of the critical current along the CC length results from its manufacturing process. This variation causes non-uniform heat generation, particularly when the coil is operated at a high fraction of the nominal critical current or when large critical current defects are present. The temperature distribution resulting from the balance between cooling and heating, in combination with the magnetic field and critical current distributions, determines whether a thermal runaway occurs. Accurately predicting the level of critical current defects that can be tolerated during conduction-cooled operation is difficult and requires a three-dimensional (3D) coupled electromagnetic and thermal simulation.**

This paper presents the results of simulations that are performed with the open-source Finite Element Quench Simulator (FiQuS) tool developed at CERN as part of the STEAM framework. The 3D coupled magnetodynamic-thermal simulations are based on the H− ϕ formulation and use thin shell approximations, a CC homogenization and conduction-cooling. The critical current can be varied along the CC length.

The effect of a single defect specified as a reduction of the critical current along the CC length is investigated in terms of the coil's ability to reach and maintain the operating conditions. The critical current and length of the defect that results in a thermal runaway are analyzed in terms of defect location in the coil. These defect locations are compared in terms of the voltage signal available for quench detection and the implications are discussed.

***Index Terms*— HTS coils, 2G HTS Conductors, finite element method, quench protection, quench propagation**

I. Introduction

RECENT advancements in high-temperature superconductor (HTS) (Re)BCO coated conductors (CC) have improved performance, reduced costs, and increased the availability of long-length conductors and manufacturing capacity. These developments make HTS CC an increasingly viable alternative to low-temperature superconductors (LTS) [1, 2]. In particle accelerators, moving away from superfluid or bath cooling for the majority of magnets could significantly reduce energy consumption and improve sustainability, particularly in machines like the Future Circular Collider [3]. However, helium gas or conduction-cooled HTS magnets require distinct design approaches to ensure stable operation and effective quench detection and protection — key topics explored in this paper. The impact of coil conduction cooling is likely considerable here, and a different conclusion could be reached when the coil is bath-cooled.

While accelerator-class HTS magnets are not yet available for comprehensive studies, certain simpler configurations, such as single-CC pancake coils, can be studied in detail and offer valuable insights into how conduction-cooled HTS magnets behave. No-insulation (NI) coils [4] have been explored, but concerns about their increased power dissipation during ramping [5, 6] and reduced field quality [7, 8] make insulated coils a more attractive option.

A challenge with HTS CCs is the variation in critical current, I_c, along their length, typically due to the manufacturing process. Local decreases in I_c, referred to as defects, are a particular concern and are routinely measured as part of quality control [9, 10]. However, determining which defects are acceptable for stable operation is complex and not straightforward. This complexity often encourages strict quality assurance specifications regarding I_c, which may reduce manufacturing yields and increase costs. Few studies have explored how to quantify acceptable I_c defects for conduction-cooled coils [11], highlighting an important gap in the research.

Recent advancements, such as the Finite Element Quench Simulator (FiQuS) [12], developed as part of CERN's STEAM [13] framework, enable the use of three-dimensional (3D) models. These 3D simulations consider the full geometry and compute a resistive voltage for quench detection under various thermal conditions, providing deeper insights into thermal runaway scenarios. FiQuS can also simulate local I_c degradation and its effects in a coupled magnetodynamic-thermal environment.

In this paper, acceptable I_c defect lengths, positions and degradation levels are presented for stable operation in

M. Wozniak, E. Schnaubelt, S. Atalay, B. Bordini, J. Dular, T. Mulder, E. Ravaioli and A. Verweij are with CERN, Meyrin, Switzerland (e-mail: mariusz.wozniak@cern.ch).

Manuscript received September 2024.

conduction-cooled coil geometry, and factors influencing the distribution of acceptable I_c defects are explored. This study focuses on finding minimum defect I_c for stable operation, in contrast to the study [23], which used defect I_c of 0 A. Finally, the efficiency of resistive voltage-based quench detection is studied in terms of defect location. While quench detection is closely tied to protection methods, this paper will not delve into the details of quench protection.

II. Pancake Coil

A single, 4 mm wide (Re)BCO CC with a copper stabilizer is considered, and its key properties are listed in Table I. The CC has 35 µm Kapton insulation applied to both sides. Material properties of Kapton used in the simulations were [14, 15].

TABLE I
KEY PARAMETERS OF THE (RE)BCO CC

Parameter	Value	Unit
I_c (15 K, 15 T)	700	A
n-value = const.	30	-
Width	4	mm
(Re)BCO thickness	2.4	µm
Hastelloy® thickness	40	µm
Copper thickness	60	µm
Silver thickness	2	µm
Copper / Silver RRR	100 / 20	-
Insulation material	Kapton	-
Insulation thickness	35	µm
Winding cell thickness	174.4	µm

As listed in Table II, a single, 20-turn pancake coil with a winding inner and outer diameter (I.D. and O.D.) and copper terminals (Fig. 1) is studied. A background magnetic field, B_b of 15 T, is applied in the axial direction. At an operating current of 500 A, the coil generates an axial central field B_{cc} of 0.5 T, and an axial peak field B_{cp} of 1.3 T. At the operating temperature T_{op} of 15 K and the coil maximum field B_{max}=B_b+B_{cp}=16.3 T, the operating current, I_{op} of 500 A, corresponds to 76% of $I_c(T_{op}, B_{max})$ of the CC.

III. Simulation Model

A. Finite Element tool

The open-source FiQuS tool is coded in Python [16] and, with the help of Gmsh [17, 18] and GetDP [19, 20], performs geometry generation, meshing, solving, and post-processing.

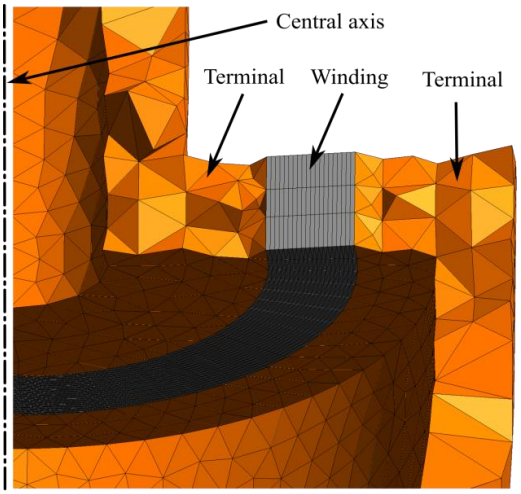

Fig. 1 Cross-section of the pancake coil mesh, with each CC meshed as 3 elements in the axial and one in the radial direction.

TABLE II
KEY PARAMETERS OF THE PANCAKE COIL

Parameter	Value	Unit
Number of turns	20	-
Winding I.D. / O.D.	20 / 26.98	mm
Terminals thickness / length	3 / 30	mm
Terminals material / RRR	Cu / 100	-
Conductor length	1.487	m
Operating current, I_{op}	500	A
Fraction of I_{op} / I_c (T_n, B_{max})	76	%
Winding cell current density at I_{op}	717	A/mm²
Operating temperature, T_{op}	15	K
Axial background field, B_b	15	T
Coil center/max field	15.5/16.3	T

The Pancake3D module of FiQuS version 2024.12.1 [21] was used with insulated coil capabilities as described in [22]. The insulation layer between the turns was simulated using the magneto-thermal thin shell approximation (TSA) [23, 24, 25]. The thermal and magnetodynamic contributions to the model behavior were adjusted to study their impact independently. By default, the magnetic field and temperature distribution are calculated in 3D, referred to as 3D cases in the following. To simulate classical 1D thermal heat diffusion in the winding, the heat flow between coil turns (i.e., across the thermal TSA) was turned off for the cases referred to as 1D in the following. Note that the heat flow modeled in the 1D case is two-dimensional since the axial heat flow is considered. The temperature gradient in the axial direction is negligible, and the thermal simulation is essentially 1D. The term 1D is used instead of 2D to highlight that this case simulates a classical 1D quench propagation. I_c was considered as either $I_c(B_b, T)$ or $I_c(B_b+B_c, T)$ for the cases with background field only or with total magnetic field.

B. $J_c(B, T)$ function

The critical current density was defined as [26]:

$$J_c(B,T) = \frac{I_{c,0}(T)}{A_{sc}}\left(1+\frac{B}{B_{0,0}(T)}\right)^{-\alpha}\left(1-\frac{B}{B_{irr,0}(T)}\right)^{-q}, \quad (1)$$

with the temperature-dependent parameters given by:

$$I_{c,0}(T) = I_{c,0,0}\left(1-\frac{T}{T_{c,0}}\right)^{\gamma}, \quad (2)$$

$$B_{0,0}(T) = B_{0,0,0}\left(1-\frac{T}{T_{c,0,0}}\right), \quad (3)$$

$$B_{irr,0}(T) = B_{irr,0,0}\left(1-\frac{T}{T_{c,0,0}}\right)^{\beta}, \quad (4)$$

with A_{sc} the cross-sectional area of the (Re)BCO layer, $I_{c,0,0}$ the critical current at zero field and temperature, $B_{0,0,0}$ the characteristic field at zero current and temperature, $B_{irr,0,0}$ the irreversibility field at zero current and temperature and $T_{c,0,0}$ the critical temperature at zero current and magnetic field, α, β, γ and q are the fitting constants.

The $J_c(B, T)$ fit was multiplied by A_{sc} to obtain $I_c(B, T)$, and a fit was performed at 0 deg (field perpendicular to the wide surface of the CC) to data of the CC manufactured by the Faraday Factory and available at [27].

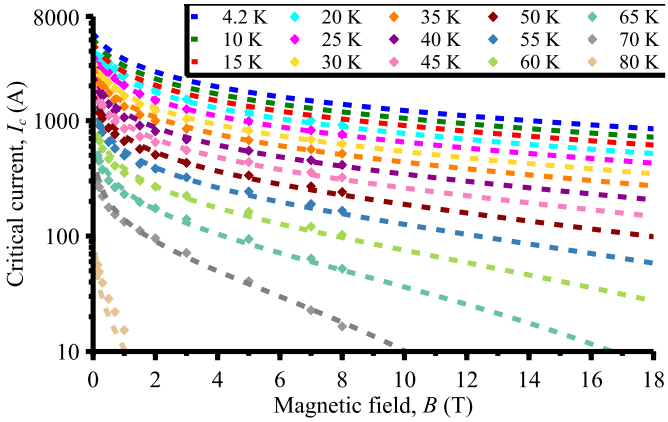

Fig. 2 Critical current as a function of magnetic field parameterized by the temperature. Measured data points are represented by markers, and the dashed lines represent the I_c (B, T) fit of eq. (1) with parameters given in Table III.

TABLE III
$J_C(B, T)$ FIT PARAMETERS OF EQUATIONS (1)-(4)

Parameter	Value	Unit
$I_{c,0,0}$	6098.7	A
$B_{0,0,0}$ / $B_{irr,0,0}$	0.5769 / 200	T
$T_{c,0,0}$	85	K
A_{sc}	9600	µm²
α / β / γ / q	0.48175 / 1.4 / 1.45 / 2.0	-

The data and the fit are plotted in Fig. 2, and the fit parameters are listed in Table III. The $J_c(B, T)$ function is open-source [28] and was compiled with CERNGetDP [29] (version 2024.11.1) and used in this study. The function can be used in other software, such as COMSOL Multiphysics, Python or MATLAB [30].

C. Powering and cooling setup

The coil was simulated by the schematic shown in Fig. 3. The current source was switched off when the coil peak temperature T_{max} reached 300 K. The coil was conduction cooled via its terminals, with their ends fixed at the operating temperature T_{op} of 15 K. The heat dissipation in the terminals was disregarded, corresponding to a superconducting shunt for the current path. The temperature gradient in the terminals between the coil and the cooling source is taken into account.

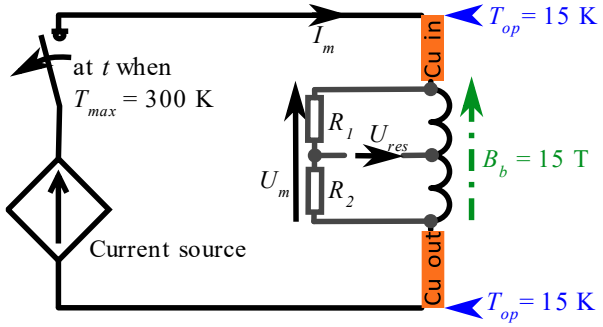

Fig. 3 Simplified schematic of the magnet electrical and thermal circuits.

D. Resistive voltage computation

The resistive component of the coil voltage is used for quench detection, achieved by using a central voltage tap (Fig. 3) with ideal compensation of the inductive voltage. To compute the resistive voltage U_{res} of the HTS CC winding as a post-processing quantity, a solid conductor winding function $\chi = -\nabla v$ with 3D support in the whole coil was computed [31]. The electric scalar potential v was calculated in each time step by solving a unitary stationary current flow problem following [32] using the conductivity values for the computed temperature and magnetic field distribution at that time step. From χ, the DC conductance G was computed. Finally, U_{res} was obtained by multiplying G with the total voltage U_m and the potential difference between the beginning and the end of the winding, i.e., the difference of values of v at those locations.

E. Defect definition

A defect is a region of the CC with a reduced critical current due to a local reduction of the (Re)BCO thickness or width. This means that the critical current of the defect, $I_{c,d}(B, T)$, is changing with field and temperature. A single defect is introduced by locally changing the parameter $I_{c,0,0}$ in eq. 2, such that the local $I_c(B_b, T_n)$ or $I_c(B_b+B_c, T)$ matches $I_{c,d}$. A constant n-value of 30 is used for the defect and the rest of the winding.

The defect length, l_d, and its central location in terms of coil turn number n_d need to be specified for a full defect definition (Fig. 4). The turn number n_d is equivalent to specifying a location along the conductor length, x, although the relation between n_d and x is nonlinear as shown in Fig. 4. The first ($n_d \in [0, 1]$) and last turn ($n_d \in [19, 20]$) are soldered to the copper terminals. Defects in these locations and up to 0.5 turns away are not considered; hence n_d is in the range from 1.5 to 18.5.

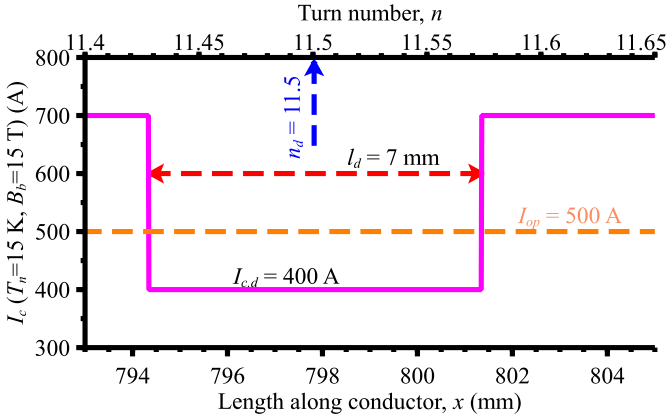

Fig. 4 Example of a critical current defect definition, assuming a 7 mm long defect at a location of turn 11.5 and with a critical current of 400 A.

IV. Results and Discussion

Section IV.A introduces the concept of the minimum stable defect critical current $I_{c,d,m}$ for fixed defect length. Next, the dependence of $I_{c,d,m}$ on n_d is examined for both 1D and 3D cases and the impact of B_c on $I_{c,d,m}$ is discussed(Section IV.B). Finally, the coil resistive voltage for quench detection is presented when $I_{c,d}$ is just below $I_{c,d,m}$. This is then compared for two defect locations, one close to the innermost turn, and the other location close to the outermost turn and the results are analyzed (section IV.C).

A. Minimum stable defect critical current

The minimum stable defect critical current, $I_{c,d,m}$, is defined as the value of $I_{c,d,}$ which allows the coil to reach its I_{op}, and operate without experiencing a thermal runaway. The $I_{c,d,m}$ is determined for coil current ramp rates that do not induce substantial AC losses, which could otherwise lead to thermal runaway during the ramp.

Fig. 5 shows the peak coil temperature at the end of the ramp to the operating current of 500 A and 1D heat flow and for defects with l_d = 7 mm at turn n_d = 11.5, and with $I_{c,d}$ of 523 and 524 A. The lower value causes a thermal runaway, whereas the coil peak temperature and total Joule power are stable for the higher $I_{c,d}$ of 524 A, which therefore corresponds to the $I_{c,d,m}$ for the l_d and n_d considered. For this 1D case, a defect of 523 A causes a thermal runaway at an operating current of 500 A. Already, for a defect with $I_{c,d}$ 23 A above the operating current, the heat dissipation due to a finite n-value and current sharing with the copper stabilizer is above what can be removed by heat conduction along the tape.

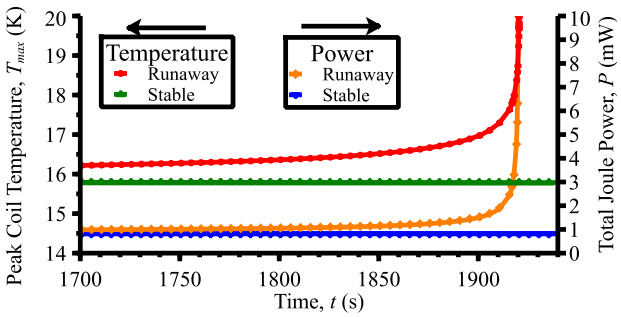

Fig. 5 Peak temperature and total Joule power in the coil with l_d = 7 mm and n_d = 11.5 for the 1D case. The stable (runaway) $I_{c,d}$ is 524 (523) A. The time range close to the runaway is shown.

B. Defect location for 1D or 3D case and coil magnetic field impact

A study of the dependence of $I_{c,d,m}$ on n_d was performed for l_d = 2 mm and 7 mm as well as 1D and 3D cases (Fig. 6). In the 1D case and l_d = 7 mm, the $I_{c,d,m}$ ranges from 484 to 524 A. The dependence on n_d is largely due to the heat conduction path length from the defect to the (cooling) terminals. The shortest length is for n_d=1.5, which results in the lowest $I_{c,d,m}$. For the 1D case, a shorter l_d of 2 mm results in a decrease of the $I_{c,d,m}$ by 17 to 25 A. On average, for all defect locations, the shorter defect causes $I_{c,d,m}$ to be lower by 21 A. The shorter the defect, the larger the decrease of the $I_{c,d,m}$ can be tolerated without a thermal runaway. The 3D case allows for heat diffusion between the turns, which further lowers the $I_{c,d,m}$ and a stable operation can be achieved with the $I_{c,d,m}$ lower on average for all defect locations by 59 A.

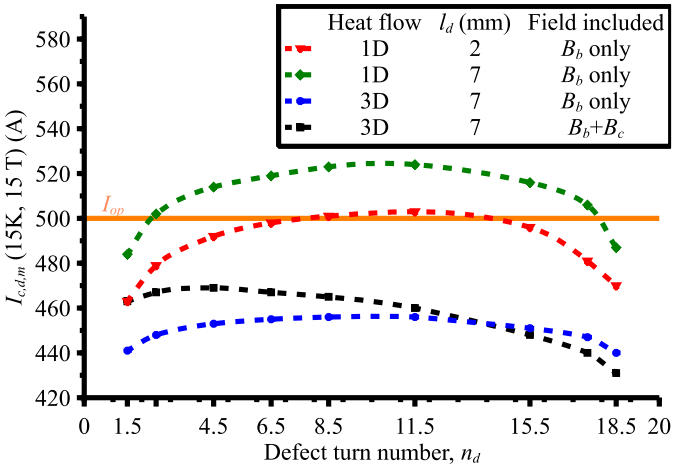

Fig. 6 Minimum stable defect critical current $I_{c,d,m}$(15 K, 15 T) for defect length l_d of 2 and 7 mm and calculated for heat flow of 1D or 3D cases and background magnetic field B_b only or with B_b and coil magnetic field B_c. Lines connecting points are for visualization only.

The most stable position, with the lowest $I_{c,d,m}$ of 440 A is now on the outer turn of the coil (n_d=18.5). In this area, heat conduction across the insulation dominates because the turn radius is larger, hence the insulation cross-section for the heat conduction. The inside of the coil (n_d=1.5) has $I_{c,d,m}$ of 441 A. The coil peak field B_{cp} is 1.3 T at I_{op}. When B_c is included together with B_b, it impacts $I_{c,d,m}$, which increases at the inner turns and decreases at the outer turns. For the inner turns, the B_c is in a similar direction as the B_b, creating a higher field, whereas for the outer turns, the B_c in in the mostly opposite direction to B_b and lowers the total field seen by the turns.

C. Quench detection and thermal runaway

To cause a thermal runaway, an $I_{c,d}$ of 1 A below the $I_{c,d,m}$ for l_d=7 mm and at locations n_d=1.5 and n_d=11.5 were chosen. Of key interest is the time from the resistive voltage exceeding the 10 mV quench detection threshold until the time when the thermal runaway is well advanced, which is taken when the

coil peak temperature exceeds 200 K.

Fig. 7 shows the last 120 ms before a thermal runaway during a current ramp to 500 A in 2400 s (40 min) for the 3D case. The voltage during the ramp steadily increased and reached 10 mV at about 41.6 ms before the thermal runaway was well advanced. This shows that there is very little time to protect the coil.

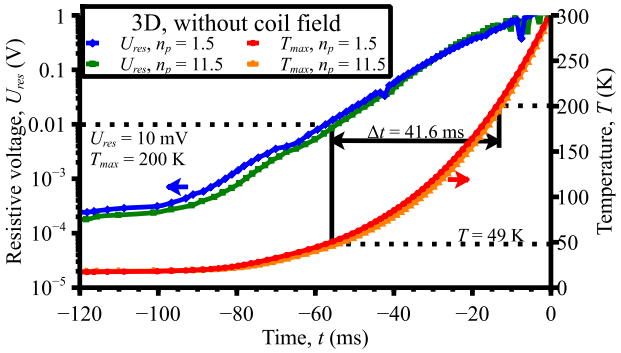

Fig. 7 Resistive voltage due to a 7-mm long defect with $I_{c,d}$ of 1 A below $I_{c,d,m}$ and location of turn n_d = 1.5 ($I_{c,d}$ = 440 A) and n_d = 11.5 ($I_{c,d}$ = 455 A) with 3D heat diffusion and background magnetic field only. The time axis was adjusted to be zero when T_{max} reached 300 K.

The voltage and temperature increase are remarkably similar for the two defect locations, indicating that most of the resistive voltage is generated by the coil turn with the defect, and the heat diffusion to the neighboring turns is not yet sufficient to heat them up and contribute substantial resistive voltage. Fig. 8 shows the temperature of the coil for the two defect locations at the time when the resistive voltage reached 10 mV. In the case of the defect at n_d=1.5 turn, the most inner turn remains at about 15 K as it is in good contact with the inner terminal (not shown). The defect at n_d=11.5 turn heats up the turns on both sides, but these turns do not contribute to the resistive voltage for quench detection.

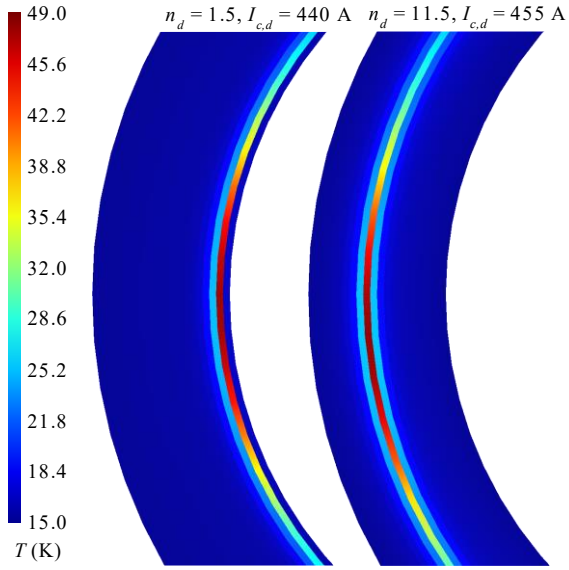

Fig. 8 Temperature distribution at times when the resistive voltage reached the quench detection threshold of 10 mV for the 3D case for the defect at n_d = 1.5 turns and $I_{c,d}$ = 440 A (left) and n_d = 11.5 turns and $I_{c,d}$ = 455 A (right).

V. Conclusion

The recently developed FiQuS tool was used to study a high-temperature superconductor coated-conductor pancake coil. The concept of minimum defect critical current was introduced, and its dependence on defect length and position within the coil, as well as the effects of 1D and 3D heat diffusion in a conduction-cooled environment, were analyzed. The influence of the coil's magnetic field on these results was also demonstrated. This approach, when applied to a specific coil, could be valuable for decision-making when determining the acceptable critical current defect based on available critical current measurements along the coated conductor length.

Additionally, it was shown that for a conduction-cooled coil with a defect leading to thermal runaway, the resistive voltage exceeds the typical quench detection threshold for a very short time of milliseconds seconds before thermal runaway occurs. This time is not significantly affected by the defect location in the coil. In this case, there is minimal time to validate the signal and activate protection measures before the peak temperature rises to critical levels. The challenges in detecting and protecting HTS coils against the consequences of a quench have been clearly demonstrated in this study.

REFERENCES

[1] D. Uglietti, "A review of commercial high temperature superconducting materials for large magnets: from wires and tapes to cables and conductors," *Supercond. Sci. Technol*, vol. 32, no. 5. IOP Publishing, p. 053001, Apr. 09, 2019. doi: 10.1088/1361-6668/ab06a2

[2] L. Rossi and C. Senatore, "HTS Accelerator Magnet and Conductor Development in Europe," *Instruments*, vol. 5, no. 1, p. 8, Feb 2021, doi: 10.3390/instruments5010008.

[3] Benedikt, M., Blondel, A., Janot, P. et al. "Future Circular Colliders succeeding the LHC," *Nat. Phys.*, vol. 16, pp. 402–407, Apr 2020., doi: 10.1038/s41567-020-0856-2

[4] S. Hahn, D. K. Park, J. Bascunan and Y. Iwasa, "HTS Pancake Coils Without Turn-to-Turn Insulation," in *IEEE Transactions on Applied Superconductivity*, vol. 21, no. 3, pp. 1592-1595, June 2011, doi: 10.1109/TASC.2010.2093492

[5] Y. Wang, H. Song, W. Yuan, Z. Jin, and Z. Hong, "Ramping turn-to-turn loss and magnetization loss of a No-Insulation (RE)Ba2Cu3Ox high temperature superconductor pancake coil," *Journal of Applied Physics*, vol. 121, no. 11, Mar. 2017, doi: 10.1063/1.497859

[6] A. Cubero, A. B. Núñez-Chico, R. Navarro, L. A. Angurel, and E. Martínez, "Electromagnetic behaviour and thermal stability of a conduction-cooled, no-insulated 2G-HTS coil at intermediate temperatures," Cryogenics, vol. 108, p. 103070, Jun. 2020, doi: 10.1016/j.cryogenics.2020.103070

[7] D. G. Yang, K. L. Kim, Y. H. Choi, O. J. Kwon, Y. J. Park, and H. G. Lee, "Screening current-induced field in non-insulated GdBCO pancake coil," *Supercond. Sci. Technol.*, vol. 26, no. 10, p. 105025, Sep 2013, doi: 10.1088/0953-2048/26/10/105025.

[8] C. Barth et al., "Generation of 25 T with an all-superconducting magnet system: field profile and field quality measurements of a layer-wound 4 T REBCO insert coil for a 21 T LTS magnet," *Supercond. Sci. Technol.*, vol. 32, no. 7, p. 075005, May 2019, doi: 10.1088/1361-6668/ab0fa

[9] S. Furtner, R. Nemetschek, R. Semerad, G. Sigl and W. Prusseit, "Reel-to-reel critical current measurement of coated conductors," *Supercond. Sci. Technol.*, vol. 17, pp. S281–S284, Mar 2004, doi: 10.1088/0953-2048/17/5/037

[10] X. -F. Li, A. B. Yahia, G. Majkic, M. Kochat, S. Kar and V. Selvamanickam, "Reel-To-Reel Critical Current Measurement of REBCO Coated Conductors," *IEEE Trans. Appl. Supercond.*, vol. 27, no. 4, pp. 1-5, June 2017, Art no. 3800205, doi: 10.1109/TASC.2016.2640942.

[11] Fedor Gömöry and Ján Šouc, "Stability of DC transport in HTS conductor with local critical current reduction," *Supercond. Sci. Technol.*, vol. 34, no. 2, Jan 2021, art. no 025005, doi: 10.1088/1361-6668/abc73e

[12] FiQuS tool. [Online]. Available: https://cern.ch/fiqus

[13] STEAM framework. [Online] Available: https://cern.ch/steam

[14] Thermal conductivity function CFUN_kKapton_v2.c. Available: https://gitlab.cern.ch/steam/steam-material-library

[15] Thermal conductivity function CFUN_CvKapton_v1.c. Available: https://gitlab.cern.ch/steam/steam-material-library

[16] Python Programming Language. [Online]. Available: https://www.python.org/

[17] Gmsh. [website]. Available: http://gmsh.info/

[18] C. Geuzaine and J.-F. Remacle, "Gmsh: A 3-D finite element mesh generator with built-in pre- and post- processing facilities," *International Journal for Numerical Methods in Engineering*, vol. 79, pp. 1309–1331, May 2009, doi: 10.1002/nme.2579

[19] GetDP [website]. Available: http://getdp.info/

[20] P. Dular, C. Geuzaine, F. Henrotte, and W. Legros, "A general environment for the treatment of discrete problems and its application to the finite element method," *IEEE Transactions on Magnetics*, vol. 34, no. 5, pp. 3395–3398, 1998. doi: 10.1109/20.717799

[21] FiQuS Python package. [Online]. Available: https://pypi.org/project/fiqus/2024.7.0

[22] S. Atalay, E. Schnaubelt, M. Wozniak, J. Dular, G. Zachou, S. Schöps and A. Verweij, "An open-source 3D FE quench simulation tool for no-insulation HTS pancake coils," Supercond. Sci. Technol., vol. 37, May 2024, art. no 065005, doi: 10.1088/1361-6668/ad3f83

[23] E. Schnaubelt, M. Wozniak and S. Schöps, "Thermal thin shell approximation towards finite element quench simulation," Supercond. Sci. Technol., vol. 36, Mar 2023, art. no 044004, doi: 10.1088/1361-6668/acbeea

[24] E. Schnaubelt, M. Wozniak, S. Schöps and A. Verweij, "Electromagnetic Simulation of No-Insulation Coils Using H – ϕ Thin Shell Approximation," *IEEE Trans. Appl. Supercond.*, vol. 33, no. 5, pp. 1-6, Aug. 2023, Art no. 4900906, doi: 10.1109/TASC.2023.3258905

[25] E. Schnaubelt *et al*., "Magneto-Thermal Thin Shell Approximation for 3D Finite Element Analysis of No-Insulation Coils," *IEEE Trans. Appl. Supercond.*, vol. 34, no. 3, pp. 1-6, May 2024, Art no. 4700406, doi: 10.1109/TASC.2023.3340648

[26] G. Succi, A. Ballarino, S. C. Hopkins, C. Barth and Y. Yang, "Magnetic Field and Temperature Scaling of the Critical Current of REBCO Tapes," *IEEE Trans. Appl. Supercond.*, vol. 34, no. 3, pp. 1-7, May 2024, Art no. 8001007, doi: 10.1109/TASC.2024.3370137

[27] High-temperature superconducting wire critical current database of Victoria University of Wellington, New Zealand. Available: https://htsdb.wimbush.eu/dataset/23536374, doi: 10.6084/m9.figshare.23536374.v4

[28] Critical current density function CFUN_HTS_JcFit_Succi_v2.c. Available: https://gitlab.cern.ch/steam/steam-material-library

[29] CERNGetDP version 2024.8.2. Available: https://cern.ch/cerngetdp

[30] STEAM materials library (SMaLi). Available: https://cern.ch/smali

[31] S. Schöps, H. De Gersem, and T. Weiland, "Winding functions in transient magnetoquasistatic field-circuit coupled simulations," *COMPEL: The International Journal for Computation and Mathematics in Electrical and Electronic Engineering*, vol. 32, no. 6, pp. 2063–2083, Nov 2013, doi: 10.1108/compel-01-2013-0004

[32] A. Alonso Rodríguez and A. Valli, "Voltage and current excitation for time-harmonic eddy-current problems," *SIAM Journal on Applied Mathematics*, vol. 68, no. 5, pp. 1477–1494, 2008.